Journal of Coastal Research	00	0	000–000	Coconut Creek, Florida	Month 0000

Hydrodynamic Conditions Associated with an Onshore Migrating and Stable Sandbar

Jun Cheng[†]*, Ping Wang[†], and Ernest R. Smith[‡]

[†]School of Geosciences
University of South Florida
Tampa, FL 33620, U.S.A.

[‡]Coastal and Hydraulic Laboratory
U.S. Army Engineer Research and Development Center
Vicksburg, MS 39180, U.S.A.

www.cerf-jcr.org

www.JCRonline.org

ABSTRACT

Cheng, J.; Wang, P., and Smith, E.R., 0000. Hydrodynamic conditions associated with an onshore migrating and stable sandbar. *Journal of Coastal Research,* 00(0), 000–000. Coconut Creek (Florida), ISSN 0749-0208.

In this study, large-scale three-dimensional laboratory data were analyzed to identify the hydrodynamic conditions associated with the onshore migration of a sandbar and the subsequent equilibrium state of a stable bar. The initial sandbar was constructed offshore and out of equilibrium, with a symmetrical shape. The bar became asymmetrical as it migrated onshore. As the rate of onshore migration slowed, the bar was restored to a symmetrical shape toward an equilibrium state. Wave and near-bottom velocity across the surf zone were measured during the onshore sandbar migration. The near-bottom velocity skewness analyzed wave by wave indicates that before the sandbar reached equilibrium, the velocity was skewed offshore in the nearshore region and was skewed onshore seaward of the bar. However, the velocity skewness pattern reversed when the beach profile reached equilibrium and the sandbar became stable. The location of maximum undertow velocity moved from nearshore to the bar crest as the sandbar evolved toward equilibrium. Furthermore, the peak onshore-directed acceleration was greater than the peak offshore-directed acceleration throughout the surf zone during the periods of both onshore migrating and stable sandbar. The maximum difference between the onshore- and the offshore-directed acceleration occurred at the seaward side of the bar crest. The analyses of the hydrodynamic conditions associated with sandbar movement in a controlled laboratory experiment provide insights on the mechanisms of sandbar migration.

ADDITIONAL INDEX WORDS: *Sandbar migration, equilibrium beach profile, undertow, velocity skewness and asymmetry, physical model.*

INTRODUCTION

Sandbars are a dynamic morphologic feature of sandy beaches. Understanding the morphodynamics of sandbars is valuable to the coastal scientific and engineering community. The trend of sandbar migration plays a crucial role for quantifying beach and dune behavior (Grunnet and Ruessink, 2005). During storm conditions, offshore sandbar migration typically occurs as a result of strong undertow associated with intense wave breaking (Thornton, Humiston, and Birkemeier, 1996). While under swell conditions, typical of a summer season, the deformed wave-orbital velocities cause the sandbar to migrate onshore (Hoefel and Elgar, 2003; Hsu, Elgar, and Guza, 2006). Under a constant wave condition, the beach profile is expected to evolve toward an equilibrium state, when the net cross-shore sediment transport rate across the profile approaches zero (Wang and Kraus, 2005). The concept of the equilibrium shape of the beach profile has proved fruitful in a variety of applications in coastal science and engineering, such as beach nourishment design and studies concerned with morphologic evolution in the nearshore (Dean, 1991). However, the mechanism for onshore sandbar migration, as well as its equilibrium state, has not been well documented.

Balance between onshore- and offshore-directed nearshore hydrodynamics at various temporal scales is critical in determining the net cross-shore sediment transport and consequently in driving onshore and offshore sandbar migration. Based on SUPERTANK laboratory data, Wang and Kraus (2005) found that the pattern of wave-energy dissipation across a large portion of the surf zone, except at the breaker line over the sandbar, becomes relatively uniform when the beach profile reaches equilibrium, as suggested by Dean (1977). As an incident wave enters shallow water, it shoals and becomes skewed, with a narrow high crest and broad low trough. This velocity skewness, which is the difference between onshore and offshore velocity, is often considered a mechanism to cause net onshore sediment transport (Roelvink and Stive, 1989). Moreover, water particles rapidly accelerate under the steep wave front and form an asymmetrical velocity pattern, resulting in onshore sediment transport (Hoefel and Elgar, 2003). Recent studies (Drake and Calantoni, 2001; Puleo *et al*., 2003) indicate that incorporating the effect of acceleration in the energetics-type sediment transport equation (Bagnold, 1963; Bailard, 1981) can significantly improve the accuracy in predicting sediment transport in comparison with the velocity-only formula. Balance between onshore sediment flux near the surface generated by velocity skewness and offshore sediment transport generated by undertow, typically below the wave-trough level, is considered the major mechanism for an equilibrium sandbar state (Stive and Wind, 1986; Svendsen, 1984). The vertical structure of undertow is influenced by breaking wave turbulence (Garcez Faria *et al*., 2000; Van Thiel de Vries *et al*., 2008). Wang *et al*. (2002) and

DOI: 10.2112/JCOASTRES-D-14-00174.1 received 16 September 2014; accepted in revision 7 February 2015; corrected proofs received 17 March 2015; published pre-print online 8 April 2015.
*Corresponding author: jun@mail.usf.edu

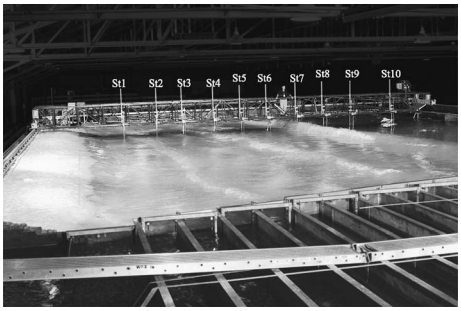

Figure 1. The LSTF during a plunging wave run, showing the instrument bridge (top) carrying current meters and wave gauges. Channels at the bottom of the photo are sediment traps to measure the sediment transport rate. The generated wave conditions are comparable to average conditions along many low-wave-energy coasts.

Wang, Smith, and Ebersole (2002) found that the cross-shore distribution pattern of undertow also is influenced by the wave breaking type (*e.g.*, plunging and spilling).

A temporal and spatial averaging scheme is often conducted to obtain rates of sediment transport (*e.g.*, Roelvink *et al.*, 2009; Van Rijn, Tonnon, and Walstra, 2011). Laboratory measurements indicate that turbulence generated by breaking waves, wave-induced currents, and sediment concentrations exhibits large temporal and spatial variations in the surf zone (Scott, Hsu, and Cox, 2009; Wang *et al.*, 2002). Thus, averaging these parameters may lead to omission of key processes important for sediment transport. Given the complicated hydrodynamic conditions associated with random wave breaking in the surf zone, a controlled laboratory environment may provide crucial insights on the hydrodynamic conditions controlling sandbar migration. A detailed analysis of hydrodynamic conditions in the surf zone with a temporal scale of individual waves in a three-dimensional (3D) laboratory environment may shed new light on the evolution of sandbars.

Based on the analyses of data collected in a large-scale sediment transport facility (LSTF), the main goals of this study are to (1) describe the hydrodynamic conditions associated with an onshore migrating and stable sandbar at a temporal scale of individual waves, (2) identify specific hydrodynamic conditions that relate to onshore sandbar migration, and (3) develop a conceptual model for sandbar evolution toward equilibrium. The high spatial and temporal resolutions allow us to investigate the change in sandbar location and geometry as the beach profile evolves toward equilibrium. Corresponding cross-shore distribution of hydrodynamic conditions such as wave breaking, velocity skewness and asymmetry, and undertow are investigated.

Experiments at the LSTF

The LSTF, located at the U.S. Army Engineer Research and Development Center in Vicksburg, Mississippi, is a large-scale 3D movable bed facility with dimensions of 30 m cross-shore, 50 m longshore, and 1.4 m high (Hamilton *et al.*, 2001). Unidirectional, long-crested irregular waves were generated by four synchronized wave generators oriented at a 10° angle with respect to the shoreline. The beach was arranged in a

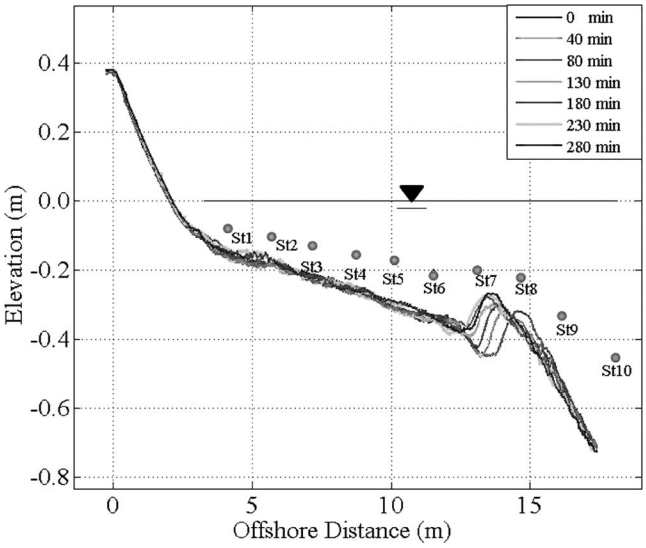

Figure 2. Time series of beach profile evolution and the location of ADV measurements. The profile is located in the middle of the wave basin. The sandbar migrated onshore during the 280-min experiment, with the bar crest moved from St8 to St7. (Color for this figure is available in the online version of this paper.)

trapezoidal plan shape corresponding to the obliquely incident waves. An external recirculation system continually recirculated currents of the same magnitude as the wave-driven longshore current through the lateral boundaries of the facility. The recirculated currents minimized adverse physical model effects at the beach boundaries and maximized alongshore uniformity of the beach, hydrodynamics, and transport rate. As the beach profile evolved, the pumps were adjusted to match the wave-driven longshore current. The longshore transport rate was uniform alongshore so that changes in the profile were not affected by longshore transport.

The fine sand ($d_{50}=0.15$ mm) beach was approximately 25 cm thick, placed over a planar concrete base, and extended 27 m alongshore and 18 m cross-shore. The incident waves generated for the bar experiments examined here had a significant height of 0.27 m and a period of 3 s. This is comparable to annual average conditions along low-wave-energy coasts, such as west–central Florida barrier islands (Wang and Beck, 2012).

The water level and current velocities (u, v, w) were measured at 10 cross-shore locations in the middle of the wave basin with synchronized capacitance wave gauges and acoustic Doppler velocimeters (ADVs), respectively (Figure 1). The velocity measurement, sampling at 20 Hz, was set equal to 10 minutes per sampling event. The velocities were measured at approximately one-third of the water depth from the bottom (Figure 2). The performance and sampling details of the instruments are described in Hamilton *et al.* (2001). The wave gauges and current meters were mounted on a steel bridge spanning the basin in the cross-shore direction. This instrument bridge can be moved and positioned precisely at different locations alongshore to measure cross-shore transects of wave and currents. The entire experiment lasted about 280 minutes

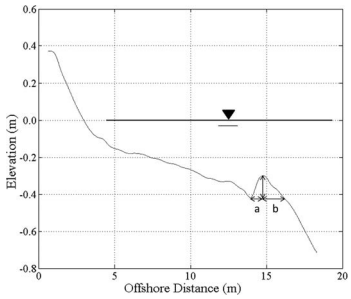

Figure 3. Parameters used to define the degree of sandbar asymmetry to quantify the morphologic evolution of the sandbar. A symmetrical sandbar has a b/a ratio of 1. The greater the b/a ratio, the more asymmetrical the sandbar is.

when the beach profile reached equilibrium, which is a state when the beach profile becomes stable (Wang *et al.*, 2002). During the experiment, the wave generators were stopped after every 40 to 50 minutes of wave action; subsequently, beach profiles were surveyed with an automated bottom-tracking profiler that traveled along the bridge. To closely associate the beach profile with the waves and currents, the wave and current measurements used here were taken at the end of each wave-run event.

METHODS

This section describes the methods used to quantify the morphology of the onshore migrating sandbar, as well as the subsequent equilibrium state. The methods used to analyze detailed hydrodynamics conditions are also discussed.

Quantifying Sandbar Morphology and Sediment Transport Rate

The sandbar is a distinctive part of a beach profile and was identified on each of the measured beach profiles. A parameter defined as b/a is used here to represent the degree of asymmetry of the sandbar, where a and b are defined in Figure 3, and a b/a ratio of 1 represents perfect symmetry. Thus, the shape of the bar and its change over time can be determined from this ratio and its temporal variation. A beach profile was surveyed every 2 m along the wave basin. Longshore variations of beach profile were small because of the alongshore uniform conditions maintained by the circulation system (Wang, Smith, and Ebersole, 2002). In the following, the beach profile surveyed in the middle of the wave basin is used.

The net sediment transport rate $\bar{q}_s$ can be calculated from the beach profile changes based on sediment mass conservation equations:

$$\frac{\partial q}{\partial x} = -(1-p)\frac{\partial z}{\partial t} \tag{1}$$

where q is the sediment transport rate, z is the bottom profile elevation, and p is the sediment porosity assumed to be homogenous and equal to 0.4 along the beach profile. The mean net sediment rate at a given cross-shore location is estimated by the following:

$$\bar{q}_s(x) = \frac{1}{\Delta t}\int_t^{t+\Delta t} q_s(x,t)dt \tag{2}$$

Identifying Wave Breaking Events

Wavelet analysis, capable of resolving rapid signal changes (Farge, 1992), is applied to detect wave breaking events from the time series of water surface elevation $X(t)$. The method proposed by Liu (2000) to detect the wave breaking event was originally applied for deep water and a finite-depth environment. The method is described in the following. Furthermore, characteristics of wave breaking under the morphologic conditions of an onshore migrating bar and a stable equilibrium profile are compared.

Liu (2000) assumed that the wave surface would break when its downward acceleration exceeded a limiting fraction γ of the gravitational acceleration g:

$$A\omega^2 > \gamma g \tag{3}$$

where A is the local wave amplitude, which can be obtained by $X(t_i) - \bar{X}$, and ω is the local wave frequency, which is computed from wavelet spectrum $X(t_i)$. Because wavelet analysis provides a local frequency spectrum for multiple scales of the wave series, the representative ω is computed as

$$\omega = \left[\frac{\int_{\omega_p}^{\omega_n} \omega^2 \Phi_i(\omega)d\omega}{\int_{\omega_p}^{\omega_n} \Phi_i(\omega)d\omega}\right]^{1/2} \tag{4}$$

in which Φ_i is the localized frequency spectrum at each time t_i, obtained from Morlet wavelet analysis (Precival and Walden, 2000) and given by

$$\Phi_i(\omega) = \left|\int_{-\infty}^{\infty} x(t_i)\psi(t_i)dt\right| \tag{5}$$

where $\psi(t)$ is the Morlet wavelet. In Equation (4), ω_n is the cutoff frequency, which is the Nyquest frequency in the LSTF (10 Hz), and ω_p is the dominant frequency. The integral interval between ω_p and ω_n suggests that it is more likely for the waves to break at the peak frequency and higher compared to those with frequencies lower than ω_p. Thus, the contribution of wave frequency in this range is accounted for in the determination of the characteristic wave frequency. The value of γ needs to be calibrated for surf zone environments, and sufficient measurements are needed to verify this approach (Liu, 2000; Liu and Babanin, 2004). The systematic measurement of the wave time series across the surf zone in the well-controlled LSTF, in addition to visual observations of wave breaking, provides a dataset to validate the method.

Wave breaking results in a wave-height decrease across the shore. To verify the overall effect of wave breaking detection by the wavelet method, the cross-shore distribution of significant wave height was examined. The significant wave height (H_{sig}) was calculated as

$$H_{\text{sig}} = 4\sqrt{\sum_1^m E(f)df} \tag{6}$$

where $E(f)$ is the power spectral density, m is the number of

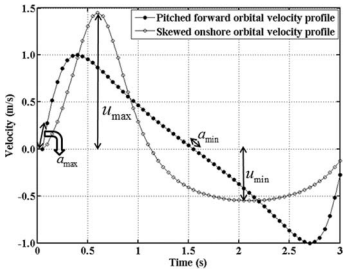

Figure 4. Synthesized, pitched forward orbital velocity profile (black line) characterized with a greater onshore-directed acceleration compared to the offshore-directed acceleration. Skewed onshore orbital velocity profile (gray line) characterized with a greater peak onshore velocity compared to the peak offshore velocity. Wave skewness plays a significant role in sandbar evolution.

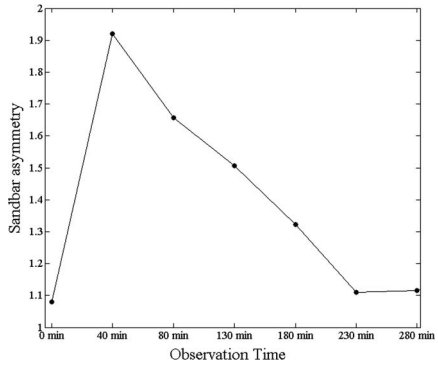

Figure 5. Evolution of the sandbar asymmetry as the bar migrated onshore. The sandbar was symmetrical at the beginning of the experiment. The bar became asymmetrical as it migrated onshore. The symmetry was reestablished as the bar reached equilibrium.

discrete Fourier frequencies in the frequency band, and df is the frequency interval over which $E(f)$ is calculated. In addition, set down and set up of the water level induced by the wave breaking was obtained by averaging the water-level measurement during the 10-minute record for both migrating and stationary sandbars.

Characteristics of Orbital Velocities

Spikes in velocity data caused by the Doppler signal aliasing, air bubble, or both can sometimes occur in ADV time-series measurements (Longo, 2006). A 3D phase space algorithm, originally developed by Goring and Nikora (2002) and validated by Mori, Suzuki, and Kakuno (2007), was applied to eliminate the spikes. The removed data points were replaced using cubic polynomial curve fitting. Only the cross-shore velocities are examined here, because the main goal is to examine the cross-shore sediment transport; the morphology alongshore is uniform because of the small incident wave angle and the circulation system. The velocity record was low pass filtered to eliminate the influence of random turbulence motion.

The skewness and asymmetry of near-bottom velocities (measured at one-third the water depth from the bottom) were examined wave by wave to identify if and how they evolve as the sandbar migrates toward equilibrium. A skewness parameter R_u for each wave is defined by Ribberink and Al-Salem (1994) as

$$R_u = \frac{u_{max}}{u_{max} - u_{min}} \tag{7}$$

where u_{max} is the largest onshore-directed velocity during one wave cycle and u_{min} is the largest offshore-directed velocity during one wave cycle (the minimum value reflects a negative number defined for offshore-directed velocity).

Using a similar approach, velocity asymmetry R_a is defined by Watanabe and Sato (2004) as

$$R_a = \frac{a_{max}}{a_{max} - a_{min}} \tag{8}$$

where a_{max} is the largest onshore-directed acceleration during one wave cycle and a_{min} is the largest offshore-directed acceleration during one wave cycle (the minimum value reflects a negative number defined for offshore-directed acceleration). The instantaneous acceleration was computed from the velocity record, sampled at 20 Hz using the finite forward difference. The parameters R_u and R_a are used to quantify the inequality between onshore and offshore velocity and acceleration, respectively. The parameters u_{max}, u_{min}, a_{max}, and a_{min} are illustrated in Figure 4. The velocity and acceleration values, instead of the R_u and R_a values, for each wave were calculated and illustrated in a box-whisker plot (Härdle and Simar, 2003). The advantage of the box-whisker plot is that it provides an overall comparison of the velocity and the acceleration between the onshore and the offshore phases of the wave, as well as among various stations.

Undertow and its cross-shore distribution, computed by averaging the 10-minute velocity record at each measurement station across the surf zone, were examined and compared during intervals when the bar was migrating onshore and was stable. As mentioned earlier, the velocity measurements were conducted at 33% of water depth from the bottom for the LSTF cases examined here. Wang *et al.* (2002) found that the peak undertow velocity was typically measured between 5 and 10 cm from the bed, or 25% to 45% of still-water depth from the bottom at most cross-shore locations. Therefore, the measurement at 33% of the water depth from the bottom used in this study should represent roughly the maximum undertow value.

RESULTS

This section discusses the morphology of an onshore migrating sandbar, as well as the subsequent equilibrium state. Hydrodynamic conditions related to the onshore migrating and equilibrium sandbar are described.

Evolution of Sandbar and Beach Profile

Time series of the measured beach profiles at the middle of the LSTF basin are illustrated in Figure 2. The beach profile reached equilibrium, defined here by a stable profile (Wang *et al.*, 2002), in approximately 5 hours (280 min) under a plunging-type breaker (Figure 1). Based on the sandbar asymmetry index defined in Figure 3, the shape of the initial

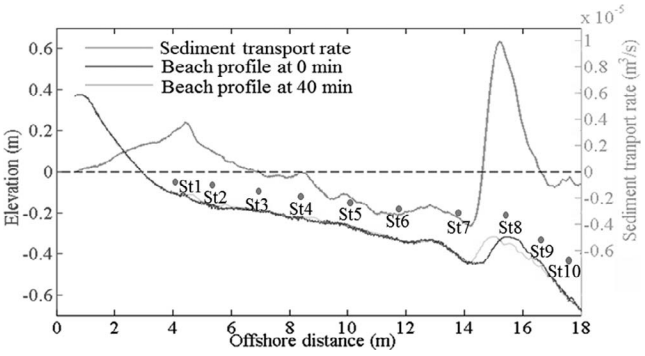

Figure 6. Cross-shore distribution of the sediment transport rate obtained from beach profile changes (the negative transport rate is directed offshore, and the positive transport rate is directed onshore). Onshore sediment transport occurred over the seaward slope of the bar, while offshore transport occurred in the middle of the surf zone. (Color for this figure is available in the online version of this paper.)

sandbar was roughly symmetrical with a value of approximately 1 (Figure 5). After the first 40 minutes of wave action, the sandbar migrated onshore and became asymmetrical, with the index reaching a maximum value of more than 1.9. As observed by various studies (Larson and Kraus, 1994; Roberts and Wang, 2012), the asymmetrical shape with a steep landward slope is indicative of an onshore migrating trend. As the sandbar continued to evolve, the degree of sandbar asymmetry decreased. The sandbar became approximately symmetrical when it reached the equilibrium state.

Most onshore sandbar migration occurred during the first 40 minutes of the experiment, as shown in Figure 2. The distribution of the cross-shore sediment transport rate calculated using Equation (2) based on beach profiles surveyed at 0 and 40 minutes is shown in Figure 6. The cross-shore sediment transport rate distribution illustrates a significant peak of onshore-directed transport just landward of the crest of the initial sandbar. A smaller peak of onshore-directed sediment transport occurred within the inner surf zone landward of the secondary breaker line. Between the secondary breaker line and the trough of the sandbar, the net sediment transport is directed offshore, with an increasing magnitude toward the trough. The longshore transport rate was uniform alongshore and did not have significant influence on beach profile evolution (Wang *et al.*, 2002). In the following, hydrodynamic analyses are conducted at a temporal scale of individual waves in an attempt to explain this particular pattern of cross-shore sediment transport associated with onshore sandbar migration.

Table 1. *Input wave condition for each wave run.*

Time (min)	Peak Period (s)	Sig Wave Height (m)
2	2.84	0.26
40	2.84	0.26
280	3.01	0.27

Sig = significant.

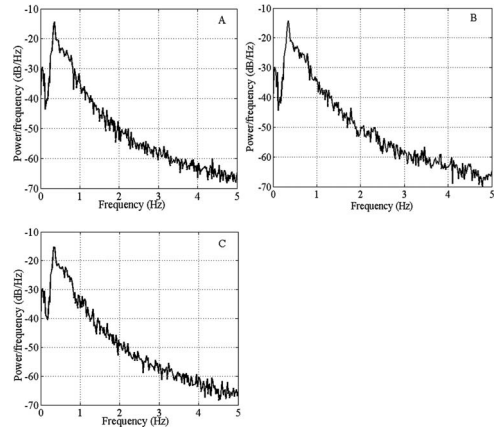

Figure 7. Wave spectrum measured at St10 (A) at the beginning of the wave run, (B) at 40 min of the wave run, and (C) at the end of the wave run. Nearly identical incident waves were measured.

Wave Breaking Associated with Onshore Sandbar Migration

The input wave condition (wave parameter at St10) for 2, 40, and 280 minutes of wave run is listed in Table 1, and its corresponding spectrum is illustrated in Figure 7. The dominant wave period is about 3 seconds, and the wave height at 280 m of the wave run is slightly greater than that of 2 and 40 minutes of wave run (Table 1). This is likely associated with wave generation instead of morphology change. Examples of

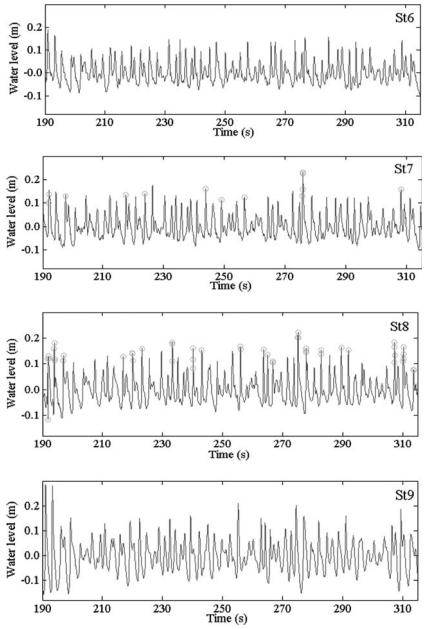

Figure 8. Example of waves measured at the beginning of the wave run at St6–St9. The circles mark breaking wave events detected by wavelet analysis at St7 and St8. The wavelet method was able to identify the breaking of high waves.

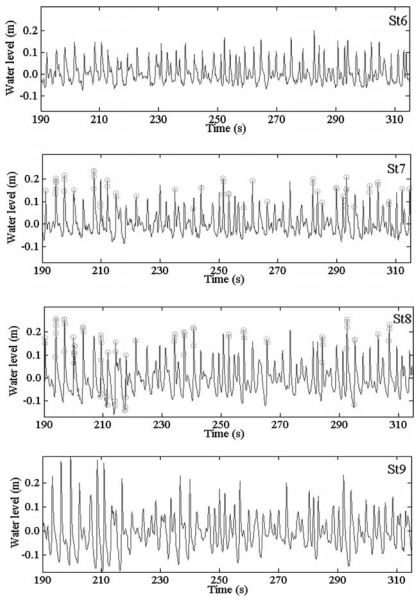

Figure 9. Example of waves measured when the sandbar reached equilibrium at St6–St9. The circles mark breaking wave events detected by wavelet analysis at St7 and St8. The wavelet method was able to identify the breaking of high waves.

wave motion measured at the beginning of the experiment and when the beach profile approached equilibrium (at 280 min) are illustrated in Figures 8 and 9, respectively. The wave deformation as it propagates landward is apparent, with a sharp crest and a broad trough. It also is apparent that the wave height decreases as the wave propagates toward the shoreline.

The landward wave-height decrease is more clearly shown in Figure 10. From St10 to St9, the wave height increased because of shoaling over the seaward slope of the sandbar. The wave height decreased sharply at St8 as a result of wave breaking for the measurement conducted at 2 and 40 minutes. For the last measurements, when the beach profile approached equilibrium, at 280 minutes the substantial wave-height decrease occurred at St7. The sandbar crest migrated from approximately St8 to St7 (Figure 2) during the equilibration process;

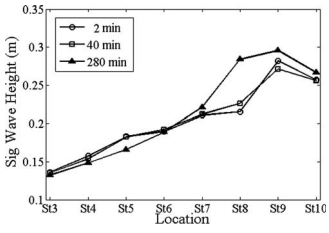

Figure 10. Distribution of significant wave height across the surf zone at different times. The onshore sandbar migration had significant influence on the wave breaking pattern, as illustrated by the onshore shift of the zone with a sharp wave-height decrease.

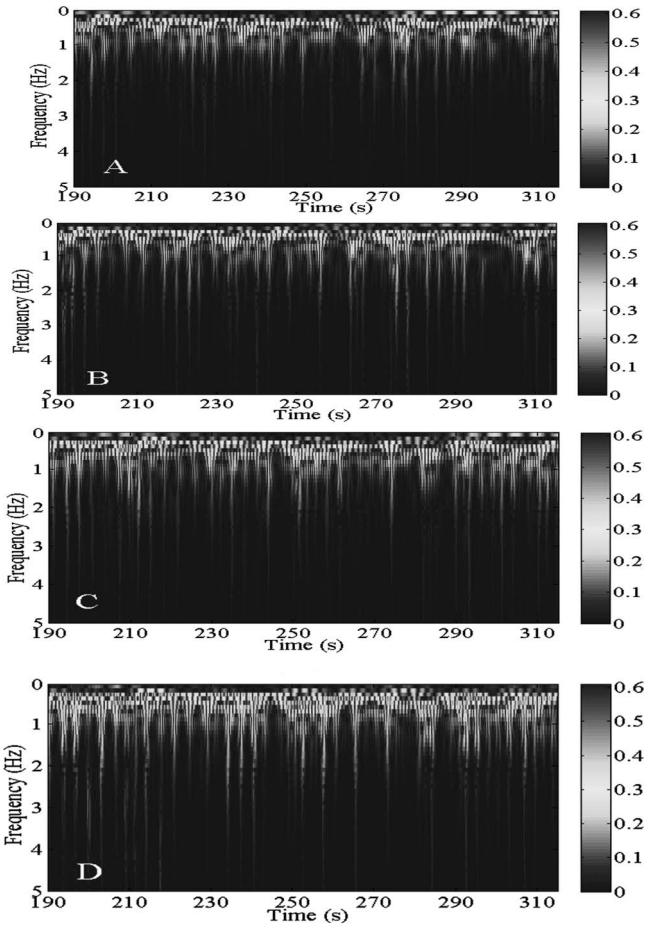

Figure 11. Time–frequency wavelet spectrum for each data point of the water-level records shown in Figures 8 and 9. The color code represents a wavelet coefficient, which is proportional to energy (A) at St7 at the beginning of the wave run, (B) at St8 at the beginning of the wave run, (C) at St7 when the sandbar reached equilibrium, and (D) at St8 when the sandbar reached equilibrium. (Color for this figure is available in the online version of this paper.)

consequently, the location of the most intensive wave breaking moved landward. This agrees with numerous studies correlating the main breaker line with the crest of the sandbar (*e.g.*, Guedes *et al.*, 2011; Pape and Ruessink, 2011).

Examples of the time–frequency wavelet spectrum computed from the wavelet analysis method developed by Liu and Babanin (2004) for each data point of the water-level time series at St7 and St8 is shown in Figure 11 to illustrate the wavelet method for wave breaking detection. The panels correspond to the dataset presented in Figures 8 (St7 and St8) and 9 (St7 and St8). The color code represents a wavelet coefficient (Liu and Babanin, 2004), which is proportional to energy. Wave breaking yields a large wavelet coefficient in the high-frequency region, illustrated in Figure 11 as spikes of the light color. This also results in a large $A\omega^2$ value (Equation (3)). Therefore, the greater the $A\omega^2$ value (in Equation (3)), the more likely the wave has broken.

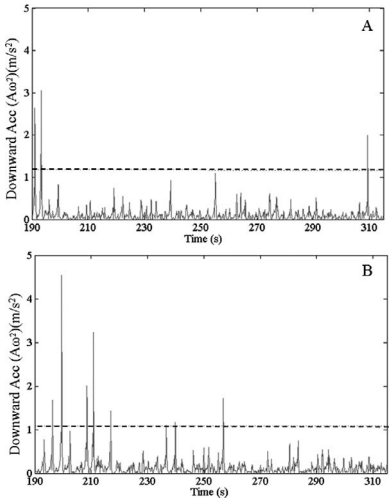

Figure 12. Downward acceleration obtained from the wavelet spectrum (A) computed from the water level measured at St9 at the beginning of the wave run and (B) computed from the water level measured at St9 when the sandbar reaches equilibrium. Because limited wave breaking occurred at St9, the data here are used to determine the threshold to detect wave breaking (dashed line).

We examine variations of wave breaking patterns associated with the bar migration. The threshold for wave breaking detection is determined as follows. Based on observations during the experiment, wave breaking rarely occurred at St9 throughout the experiment. An example of the time series of $A\omega^2$ at St9 is illustrated in Figure 12, with a dashed line drawn at the 99.5 percentile of $A\omega^2$ (approximately equal to 1 in this case) of the entire record. The values above the line are considered outliers and likely represent occasional wave breaking events.

The major wave breaking location is identified by comparing the 99.5 percentile value for all stations across the surf zone (Figure 13). The highest value was obtained at St8, indicating that major wave breaking occurred at this location, which is consistent with the sharp wave-height decrease for the measurements at 2 and 40 minutes (Figure 10). Thus, the general pattern of wave breaking illustrated by wave-energy dissipation is consistent with the results from the wavelet analysis. At 280 minutes, when the beach profile has approached equilibrium, the most intense wave breaking occurred at St7 (Figure 10), as indicated by the sharp wave-height decrease. However, a substantial peak still occurred at St8, indicating that at equilibrium, occasional high waves still broke at St8, resulting in the large $A\omega^2$ value.

Using a threshold value of 1 to determine the initiation of wave breaking, the value of γ (Equation (3)) is approximately 0.1, which is smaller than the value of 0.4 suggested by Hwang, Xu, and Wu (1989) for breaking waves. However, Holthuijsen and Herbers (1986) suggest that the value of γ should be smaller than 0.4. Liu and Babanin (2004) emphasized that the value of γ requires verification with data.

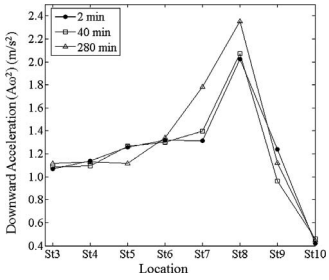

Figure 13. Wave breaking determined based on wavelet analysis. Major wave breaking occurred at St8 at the beginning of the experiment. The breaker zone became wider, extending from St8 to St7, after the sandbar reached equilibrium.

The breaking wave events identified by the wavelet method are labeled with red markers on the raw water-level record shown in Figures 8 and 9. In general, the wave breaking markers coincide with high waves, which is expected. At the beginning of the experiment, most wave breaking occurred at St8, whereas wave breaking at St7 was sparse. When the beach profile approached equilibrium, frequent wave breaking occurred at both St7 and St8. This is also illustrated by the large $A\omega^2$ values at St7 and St8 at equilibrium (Figure 13). Figures 8 and 9 also illustrate breaking of groups of high waves. The active wave breaking identified at St7 and St8 suggests that as the sandbar reached equilibrium, major wave breaking occurred over a wider zone compared to a narrower zone (at St8) over the initial out-of-equilibrium sandbar. This is consistent with visual observation during the experiment.

Wave-Induced Hydrodynamics Associated with Sandbar Migration and Equilibration

The values of $u_{\max}$, $u_{\min}$, $a_{\max}$, and $a_{\min}$ derived from the near-bottom velocity wave by wave across the surf zone are illustrated in Figure 14. The onshore-directed acceleration is greater than the offshore-directed acceleration throughout the entire equilibration process and at all measurement stations in the breaking zone, with the largest differences occurring at St9 and St8, as shown in Figure 14B. At the beginning of the experiment, St8 was located at the sandbar crest and St9 was over the seaward slope of the sandbar. When the beach profile reached equilibrium, St7 was located closer to the sandbar crest and St8 was over the seaward slope of the sandbar. The location with the maximum difference between onshore and offshore acceleration (velocity asymmetry) is closely related to the location of the sandbar crest, which agrees with findings of Hoefel and Elgar (2003) that the maximum difference is near the bar crest. The LSTF data further suggest that maximum acceleration occurs over the seaward slope of the sandbar, instead of directly over the crest.

The velocity skewness, which is the difference between onshore and offshore velocity, suggests an opposite pattern between the onshore migrating and the equilibrium sandbar, as illustrated by Figure 14A1 and A3. When the sandbar was migrating onshore, the offshore-directed velocity was generally

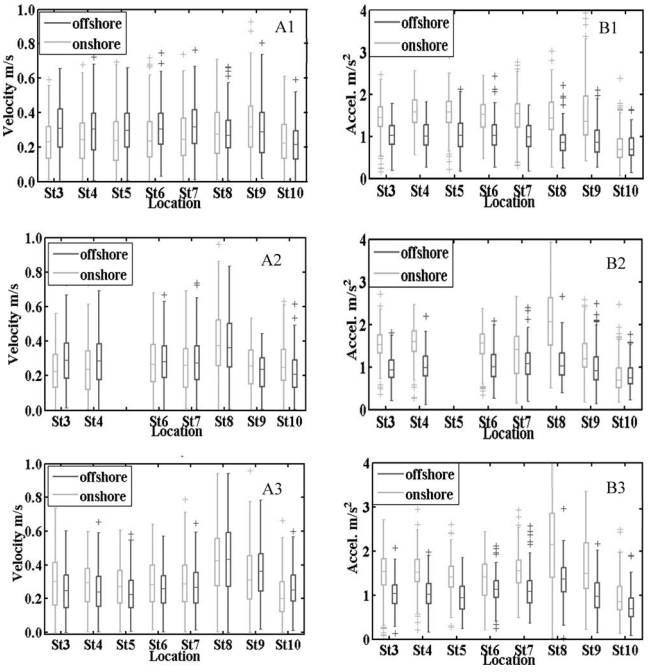

Figure 14. (A) Cross-shore distribution of maximum and minimum cross-shore velocity corresponding to (1) 2, (2) 40, and (3) 280 min. (B) Cross-shore distribution of maximum and minimum acceleration corresponding to (1) 2, (2) 40, and (3) 280 min. During onshore sandbar migration, the near-bottom orbital velocity was skewed toward offshore in the nearshore region and skewed toward onshore at and seaward of the sandbar. The opposite pattern was measured when the beach profile reached equilibrium and the sandbar stabilized. Throughout the equilibration process, the acceleration of near-bottom orbital velocity is directed dominantly onshore. (Color for this figure is available in the online version of this paper.)

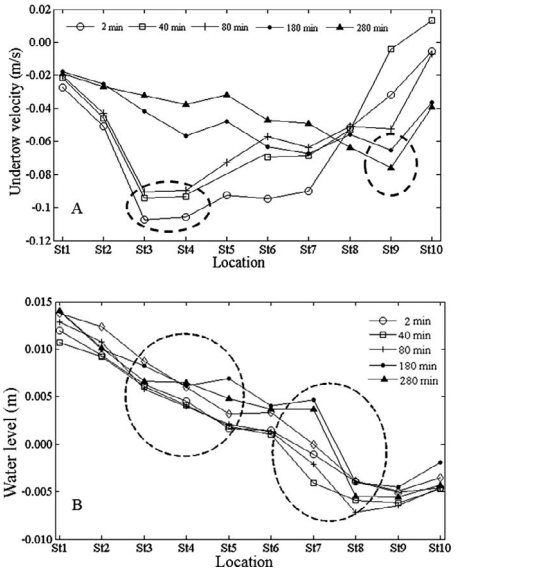

Figure 15. (A) Time-series variations of undertow distribution as the sandbar evolves toward equilibrium. (B) Time-series variations of water-level distribution across the surf zone. The peak undertow velocity shifted seaward in association with onshore sandbar migration. This is caused by varying patterns of water-level setup across the shore.

greater than the onshore-directed velocity in the nearshore region (St3–St7 in Figure 14A1), while the onshore-directed velocity was greater than the offshore-directed velocity seaward of the sandbar (St9 and St10 in Figure 14A1). This pattern of near-bottom velocity skewness largely matches the sediment transport rate distribution illustrated in Figure 6. The greater offshore velocity in the nearshore zone transported sediment toward the sandbar, whereas the onshore skewed velocity, as well as acceleration, transported sediment onshore over the seaward slope of the sandbar. When the sandbar reached equilibrium, the opposite pattern was measured, with the onshore-directed velocity greater than the offshore-directed velocity in the nearshore zone (St3–St7 in Figure 14A3) and the offshore-directed velocity greater over the seaward slope of the sandbar. The latter suggests divergence of the flow, whereas the former suggests flow convergence.

DISCUSSION

This section discusses the mechanism responsible for the velocity skewness (the difference between onshore and offshore velocity) evolution corresponding to the onshore migrating and stable sandbar. A conceptual model for sandbar evolution toward equilibrium is proposed.

Near-Bottom Velocity Skewness and Onshore Bar Migration

When the bar was out of equilibrium at the beginning of the experiment, the near-bottom cross-shore velocity was skewed offshore in the inner surf zone and skewed onshore over the seaward slope of the bar (Figure 14A1). When the profile reached equilibrium, the velocity was skewed onshore in the inner surf zone and offshore seaward of the bar. This is caused by evolution of the undertow as the beach profile changed. The seaward-directed undertow contributed to the (offshore-directed) skewness of orbital velocities. Therefore, the velocity skewness is influenced by the location of the maximum undertow. As the sandbar migrated onshore, the maximum undertow velocity location migrated from the nearshore region to just seaward of the sandbar (Figure 15A). This undertow pattern and its evolution can be explained by the time-series change of mean water level, *i.e.* setup and set-down patterns (Figure 15B). At the beginning of the experiment (2 min), the bar was far out of equilibrium and the water-level gradient in the nearshore region was greater than that at equilibrium (280 min), which drove the stronger undertow measured in the nearshore region. In the sandbar region, the water-level gradient was greater when the beach profile reached equilibrium at 280 minutes, which generated a strong undertow current at the crest and just seaward of the sandbar. The offshore migration of the peak undertow as the bar migrated onshore resulted in the change of velocity skewness.

The corresponding change of near-bottom velocity skewness as the bar migrates onshore suggests that velocity

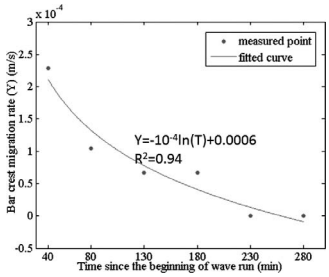

Figure 16. Change of the onshore migration rate of the sandbar with respect to time. The decreasing rate of onshore migration can be modeled by a logarithmic curve.

skewness plays an important role in controlling the migration of the sandbar. In contrast, the dominance of onshore-directed acceleration over offshore-directed acceleration (Figure 14B) throughout the profile equilibration process indicates that instantaneous water particle acceleration is not as sensitive to bar migration as is velocity skewness. Parameterization of the skewness of near-bottom velocity based on statistical wave conditions has been conducted by various studies (*e.g.*, Elfrink, Hanes, and Ruessink, 2006; Ruessink, Ramaeker, and Van Rijn, 2012) and implemented in morphologic modeling, *e.g.*, the CROSMOR cross-shore profile model (Van Rijn, Tonnon, and Walstra, 2011) and XBeach model (Roelvink *et al*., 2009). The laboratory results here support the general application of velocity skewness in modeling profile evolution. The results here also suggest that time-series evolution of velocity skewness and undertow plays an important role in the onshore migration of the sandbar.

Sandbar Evolution toward Equilibrium

The rate of onshore sandbar migration throughout the experiment varied with time. Here, the sandbar migration rate is defined as the distance of bar-crest movement over time. The variation of the migration rate over time is illustrated in Figure 16. The migration rate is the greatest during the first 40 minutes of the experiment, followed by a logarithmic decreasing trend. The rate of sandbar-crest migration can be reproduced by the logarithmic model shown in Figure 16.

The logarithmic pattern has been widely identified in coastal geomorphologic evolution and used in morphology modeling, such as the reservoir model by Kraus (2000). A logarithmic approach toward the equilibrium profile was also employed by Brutsché *et al*. (2014) in a field study of the evolution of an artificial bar-shaped nearshore berm toward an equilibrium shape. Brutsché *et al*. (2014) found that the symmetrical bell-shaped artificial nearshore berm evolved rapidly to a highly asymmetrical shape with a steep landward slope, similar to that observed in the present study.

In reality, the onshore migration rate of the artificial bar is also influenced by wave energy. The initial sandbar in this study was created during a previous experiment with higher-incident waves, and the bar migrated onshore under the smaller-input wave conditions. The LSTF data suggests that the sandbar approaches a new equilibrium state relatively quickly, on the order of a few hours.

The equilibrium state of the sandbar depends on the balance among several processes. A conceptual model for the transition from an onshore-migrating to a stable sandbar is proposed here based on the observations of hydrodynamic conditions at both time-averaged and individual wave scales. As the sandbar migrates onshore, the cross-shore pattern of time-averaged water level (*i.e.* wave setup and set-down) evolved from an approximate linear trend to a pattern with a large gradient from the bar crest to the seaward slope. This change in time-averaged water-level gradient affected the cross-shore distribution of the undertow current, which in turn alters the skewness of the near-bottom orbital velocities. Thus, a feedback mechanism exists between sandbar migration and hydrodynamics conditions. Based on the long-term bathymetric and hydrodynamic survey conducted at the U.S. Army Corps of Engineers Field Research Facility, Plant, Freilich, and Holman (2001) suggest that the feedback mechanism drive bar crests toward an equilibrium position at the wave breakpoint, which is consistent with the finding of this study.

The LSTF data suggests that onshore sandbar migration is caused by the following mechanisms: (1) offshore-directed sediment transport in the inner surf zone, associated with offshore skewed near-bottom velocity; (2) onshore-directed sediment transport at and seaward of the sandbar, associated with onshore skewed near-bottom velocity; and (3) greater onshore-directed acceleration throughout the breaking zone compared to offshore-directed acceleration. When the sandbar reached equilibrium and was stabilized, the velocity skewness pattern reversed, *i.e.* onshore skewed velocity in the nearshore zone and offshore skewed velocity at and seaward of the bar. However, onshore-directed acceleration remained greater than offshore-directed acceleration, likely providing a balancing mechanism for the stable bar.

CONCLUSIONS

Onshore sandbar migration and its driving mechanism were examined based on a large-scale 3D laboratory experiment. Concurrent measurements of nearshore hydrodynamics and beach morphology allow us to investigate the mechanisms of onshore sandbar migration. Distinctive hydrodynamic characteristics associated with an onshore migrating and a stable sandbar were identified.

The following conclusions were reached. Initially, the symmetrical sandbar became highly asymmetrical, with a steep landward slope, as the bar migrated onshore. The degree of asymmetry reduced as the beach and the sandbar approached equilibrium. Wavelet analysis is applicable to detection of wave breaking in the surf zone environment. Wave breaking is closely related to the location of the sandbar. When the sandbar reach equilibrium, major wave breaking occurred over a wider zone compared to the narrower zone over the initial out-of-equilibrium sandbar.

When the bar was migrating onshore, the near-bottom orbital velocity was skewed toward offshore in the nearshore region and skewed toward onshore at and seaward of the sandbar. The opposite pattern was measured when the beach profile reached equilibrium and the sandbar stabilized. Cross-shore distribution of time-averaged water level and undertow varied as the sandbar evolved toward equilibrium. Throughout the equilibration process, the acceleration of near-bottom orbital velocity is directed dominantly onshore, with a maximum difference between onshore- and offshore-directed acceleration occurring on the seaward slope of the sandbar.

ACKNOWLEDGMENTS

This study is jointly funded by the U.S. Army Engineer Research and Development Center and the graduate school of the University of South Florida. Permission to publish this paper was granted by the Headquarters, U.S. Army Corps of Engineers.

LITERATURE CITED

Bagnold, R.A., 1963. Mechanics of marine sedimentation. *In:* Hill, M.N. (ed.), *The Sea*. New York: Wiley-Interscience Press, pp. 507–528.

Bailard, J.A., 1981. An energetics total load sediment transport model for a plane sloping beach. *Journal of Geophysical Research,* 86(C11), 938–954.

Brutsché, K.E.; Wang, P.; Beck, T.M.; Rosati, J.D., and Legault, K.R., 2014. Morphological evolution of a submerged artificial nearshore berm along a low-wave microtidal coast, Fort Myers Beach, west–central Florida, USA. *Coastal Engineering,* 91, 29–44.

Dean, R.G., 1977. *Equilibrium Beach Profiles: U.S. Atlantic and Gulf Coasts*. Newark, Delaware: University of Delaware, Department of Civil Engineering, *Ocean Engineering Report 12*, 45p.

Dean, R.G, 1991. Equilibrium beach profiles: Characteristics and applications. *Journal of Coastal Research,* 7(1), 53–84.

Drake, T.G. and Calantoni, J., 2001. Discrete particle model for sheet flow sediment transport in the nearshore. *Journal of Geophysical Research,* 106(C9), 19859–19868.

Elfrink, B.; Hanes, D.M., and Ruessink, B.G., 2006. Parameterization and simulation of near bed orbital velocities under irregular waves in shallow water. *Coastal Engineering,* 53(11), 915–927.

Farge, M., 1992. Wavelet transform and their application to turbulence. *Annual Review of Fluid Mechanics,* 24, 395–458.

Garcez Faria, A.F.; Thornton, E.B.; Lippmann, T.C., and Stanton, T.P., 2000. Undertow over a barred beach. *Journal of Geophysical Research,* 105(C7), 16999–17010.

Goring, D.G. and Nikora, V.I., 2002. Despiking acoustic Doppler velocimeter data. *Journal of Hydraulic Engineering,* 128(1), 117–126.

Grunnet, N.M. and Ruessink, B.G., 2005. Morphodynamic response of nearshore bars to a shoreface nourishment. *Coastal Engineering,* 52(2), 119–137.

Guedes, R.M.C.; Calliari, L.J.; Holland, K.T.; Plant, N.G.; Pereira, P.S., and Alves, F.N.A., 2011. Short-term sandbar variability based on video imagery: Comparison between time-average and time-variance techniques. *Marine Geology,* 289(1–4), 122–134.

Hamilton, D.G.; Ebersole, B.A; Smith, E.R., and Wang, P., 2001. *Development of a Large Scale Laboratory Facility for Sediment Transport Research*. Vicksburg, Mississippi: U.S. Army Engineer Research and Development Center, *Technical Report ERDC/CHL TR-01-22*, 158p.

Härdle, W. and Simar, L., 2003. *Applied Multivariate Statistical Analysis*. Berlin, Germany: Springer-Verlag, 486p.

Hoefel, F. and Elgar, S., 2003. Wave-induced sediment transport and sandbar migration. *Science,* 299(5614), 1885–1887.

Holthuijsen, L.H. and Herbers, T.H.C., 1986. Statistics of breaking waves observed as whitecaps in the open sea. *Journal of Physical Oceanography,* 16(2), 290–297.

Hsu, T.J.; Elgar, S., and Guza, R.T., 2006. Wave induced sediment transport and onshore sandbar migration. *Coastal Engineering,* 53(10), 817–824.

Hwang, P.A.; Xu, D., and Wu, J., 1989. Breaking of wind-generated waves: Measurements and characteristics. *Journal of Fluid Mechanics,* 202, 177–200.

Kraus, N.C., 2000. Reservoir model of ebb-tidal shoal evolution and sand bypassing. *Journal of Waterway, Port, Coastal, and Ocean Engineering,* 126(3), 305–313.

Larson, M. and Kraus, N., 1994. Temporal and spatial scales of beach profile change, Duck, North Carolina. *Marine Geology,* 117(1–4), 75–94.

Liu, P.C., 2000. Wavelet transform and new perspective on coastal and ocean engineering data analysis. *In:* Liu, P.L.F. (ed.), *Advances in Coastal and Ocean Engineering*. Singapore: World Scientific, pp. 57–101.

Liu, P.C. and Babanin, A., 2004. Using wavelet spectrum analysis to resolve breaking events in the wind wave time series. *Annales Geophysicae,* 22, 3335–3345.

Longo, S., 2006. The effect of air bubbles on ultrasound velocity measurement. *Experiments in Fluids,* 41(4), 593–602.

Mori, N.; Suzuki, T., and Kakuno, S., 2007. Noise of acoustic Doppler velocimeter data in bubbly flows. *Journal of Engineering Mechanics,* 133(1), 122–125.

Pape, L. and Ruessink, B.G., 2011. Neural-network predictability experiments for nearshore sandbar migration. *Continental Shelf Research,* 31(9), 1033–1042.

Plant, N.G.; Freilich, M.H., and Holman, R.A., 2001. Role of morphologic feedback in surf zone sandbar response. *Journal of Geophysical Research,* 106(C1), 973–989.

Precival, D.B. and Walden, A.T., 2000. *Wavelet Methods for Time Series Analysis*. Cambridge, United Kingdom: Cambridge University Press, 569p.

Puleo, J.A.; Holland, K.T.; Plant, N.G.; Slinn, D.N., and Hanes, D.M., 2003. Fluid acceleration effects on suspended sediment transport in the swash zone. *Journal of Geophysical Research,* 108(C11), 3350–3361.

Ribberink, J.S. and Al-Salem, A.A., 1994. Sediment transport in oscillatory boundary layers in cases of rippled beds and sheet flow. *Journal of Geophysical Research,* 99(C6), 12707–12727.

Roberts, T.M. and Wang, P., 2012. Four-year performance and associated controlling factors of several beach nourishment projects along three adjacent barrier islands, west–central Florida, USA. *Coastal Engineering,* 70, 21–39.

Roelvink, J.A.; Reniers, A.J.H.M.; Van Dongeren, A.R.; Van Thiel de Vries, J.S.M.; McCall, R.T., and Lescinski, J., 2009. Modeling storm impacts on beaches, dunes and barrier islands. *Coastal Engineering,* 56(11–12), 1133–1152.

Roelvink, J.A. and Stive, M.J.F., 1989. Bar-generating cross-shore flow mechanisms on a beach. *Journal of Geophysical Research,* 94(C4), 4785–4800.

Ruessink, B.G.; Ramaeker, G., and Van Rijn, L.C., 2012. On the parameterization of the free-stream non-linear wave orbital motion in nearshore morphodynamic models. *Coastal Engineering,* 65, 56–63.

Scott, N.V.; Hsu, T.J., and Cox, D., 2009. Steep wave, turbulence, and sediment concentration statistics beneath a breaking wave field and their implications for sediment transport. *Continental Shelf Research,* 29(20), 2303–2317.

Stive, M.J.F. and Wind, H.G., 1986. Cross shore mean flow in the surf zone. *Coastal Engineering,* 10(4), 325–340.

Svendsen, I.A., 1984. Mass flow and undertow in a surf zone. *Coastal Engineering,* 8, 347–365.

Thornton, E.B.; Humiston, R.T., and Birkemeier, W.A., 1996. Bar/trough generation on a natural beach. *Journal of Geophysical Research,* 101(C5), 12097–12110.

Van Rijn, L.C.; Tonnon, P.K., and Walstra, D.J.R., 2011. Numerical modeling of erosion and accretion of plane sloping beaches at different scales. *Coastal Engineering,* 58(7), 637–655.

Van Thiel de Vries, J.S.M.; van Gent, M.R.A.; Walstra, D.J.R., and Reniers, A.J.H.M., 2008. Analysis of dune erosion process in large-scale flume experiments. *Coastal Engineering,* 55(12), 1028–1040.

Wang, P. and Beck, T.M., 2012. Morphodynamics of an anthropogenically altered dual-inlet system: John's Pass and Blind Pass, west–central Florida, USA. *Marine Geology,* 291–294(1), 162–175.

Wang, P.; Ebersole, B.; Smith, R.E., and Johnson, B.D., 2002. Temporal and spatial variations of surf-zone currents and suspended sediment concentration. *Coastal Engineering,* 46(3), 175–211.

Wang, P. and Kraus, N., 2005. Beach profile equilibrium and patterns of wave decay and energy dissipation across the surf zone elucidated in a large-scale laboratory experiment. *Journal of Coastal Research,* 21(3), 522–534.

Wang, P.; Smith, E.R., and Ebersole, B.A., 2002. Large-scale laboratory measurement of longshore sediment transport under spilling and plunging breakers. *Journal of Coastal Research,* 18(1), 118–135.

Watanabe, A. and Sato, S., 2004. A sheet-flow transport rate formulations for asymmetric, forward-leaning waves and currents. *Proceedings of 29th International Conference on Coastal Engineering* (New York), pp. 1703–1714.